

Evaluating Fisheye-Compatible 3D Gaussian Splatting Methods on Real Images Beyond 180° Field of View

Ulas Gunes¹, Matias Turkulainen², Juho Kannala^{2,3}, and Esa Rahtu¹

¹ Tampere University, Tampere, Finland

{ulas.gunes, esa.rahtu}@tuni.fi

² Aalto University, Espoo, Finland

{matias.turkulainen, juho.kannala}@aalto.fi

³ University of Oulu, Oulu, Finland

Abstract. We present the first evaluation of fisheye-based 3D Gaussian Splatting methods—Fisheye-GS and 3DGUT—on real images with fields of view exceeding 180°. Our study covers both indoor and outdoor scenes captured with 200° fisheye cameras and analyzes how each method handles extreme distortion in real-world settings. We evaluate performance under varying fields of view (200°, 160°, and 120°) to study the tradeoff between peripheral distortion and spatial coverage. Fisheye-GS benefits from field of view (FoV) reduction, particularly at 160°, while 3DGUT remains stable across all settings and maintains high perceptual quality at the full 200° view. To address the limitations of SfM-based initialization, which often fails under strong distortion, we propose a depth-based strategy using UniK3D predictions from only 2–3 fisheye images per scene. Although UniK3D is not trained on real fisheye data, it produces dense point clouds that enable reconstruction quality on par with SfM, even in difficult scenes with fog, glare, or sky. Our results highlight the practical viability of fisheye-based 3DGS methods for wide-angle 3D reconstruction from sparse and distortion-heavy image inputs.

Keywords: Fisheye · 3D Gaussian splatting · Depth Initialization

1 Introduction

3D Gaussian Splatting (3DGS) has become a foundational technique for high-quality 3D scene reconstruction and real-time image-based rendering, with widespread adoption in both academia and industry settings. Many methods have extended 3DGS to improve rendering, editing, and optimization capabilities, but almost all rely on narrow field-of-view perspective cameras, which remain the default due to their simpler design and well-established calibration pipelines.

In contrast, fisheye cameras offer ultra-wide fields of view, which allows for larger scene coverage with fewer images. This makes them highly attractive for 3D reconstruction tasks in domains such as autonomous driving, robotic perception, and virtual/augmented reality, where minimizing sensor count and capture

time is critical. By reducing the number of required viewpoints, fisheye imagery can significantly reduce the computational, memory, and time demands of reconstruction pipelines. Despite this potential, fisheye-based 3D reconstruction remains underexplored, mainly due to the additional complexity introduced by their nonlinear projection model and strong radial distortions—challenges that are largely absent in perspective setups.

To address this gap, recent methods such as Fisheye-GS and 3DGUT have adapted Gaussian splatting to work with fisheye images. These approaches modify the rendering and projection stages to support non-linear camera models, enabling native operation on wide-angle data. While promising, their real-world performance across different fields of view and indoor and outdoor scene types has not yet been systematically evaluated.

Another major obstacle lies in the initialization of the 3DGS pipeline. Traditional point cloud generation via Structure-from-Motion (SfM) is unreliable for fisheye imagery, as it assumes perspective projections and struggles with distortion-heavy input. As an alternative, monocular depth estimation offers a lightweight and sensor-free solution. However, most models are built for perspective images and do not generalize to fisheye data. UniK3D [18] is the only recent monocular estimator that supports arbitrary camera models, including fisheyes—but even it has not been trained on real fisheye imagery, largely due to the lack of datasets with aligned ground-truth depth. This makes its practical performance on real wide-angle data uncertain.

To investigate this, we explore whether monocular depth estimation can serve as a reliable alternative to traditional initialization in fisheye-based 3DGS pipelines. Specifically, we evaluate how well UniK3D predictions—despite being trained without supervision on real fisheye data—can replace SfM-generated point clouds for initializing splatting pipelines that support non-linear projection models. Our goal is not only to test compatibility but also to assess whether monocular depth is sufficiently accurate and dense to drive high-quality reconstruction across different real-world scenes.

Contributions We conduct the first evaluation of fisheye-adapted 3D Gaussian Splatting methods—Fisheye-GS and 3DGUT—on real images with fields of view exceeding 180°, across both indoor and outdoor scenes. We provide the first empirical analysis of UniK3D on real fisheye data with ultra-wide fields of view and test its effectiveness as an alternative to SfM-based initialization. We show that monocular depth from just 2–3 fisheye images per scene produces dense point clouds that lead to reconstruction quality comparable to SfM. We evaluate how reducing the field of view affects reconstruction quality and analyze the tradeoff between peripheral distortion and scene coverage. We also align the monocular point clouds to the COLMAP coordinate frame for compatibility with existing 3D Gaussian Splatting pipelines.

2 Related Work

2.1 Novel View Synthesis and 3D Gaussian Splatting

Novel view synthesis is a central task in 3D vision and graphics, aiming to generate realistic images from unseen viewpoints using a set of input images. Neural Radiance Fields (NeRF) [16] introduced a major shift by modeling scenes as volumetric radiance fields optimized through differentiable rendering. NeRF and its variants achieve high-quality results but are computationally demanding, with long training times and slow inference due to volumetric ray marching.

3D Gaussian Splatting (3DGS) [10] addresses these limitations with an alternative scene representation. It models geometry as a set of anisotropic Gaussians in 3D space, each storing appearance and opacity. These Gaussians are rasterized directly during rendering, bypassing ray marching and enabling real-time performance while maintaining photorealistic quality. The method supports continuous optimization of both geometry and appearance through gradient descent, which makes it well-suited for reconstruction pipelines.

Most 3DGS pipelines are designed for narrow field-of-view perspective images. They typically require many input views to ensure sufficient scene coverage and parallax. Initialization depends on a Structure-from-Motion (SfM) stage, commonly implemented using COLMAP [19], which estimates camera poses and sparse geometry from multiview correspondences. Although COLMAP supports fisheye models, such as OpenCV’s fisheye camera [1], its parameter estimates can become unreliable under strong distortion or very wide fields of view. Accurate results often require pre-calibrated intrinsics. This introduces additional steps and assumes access to the physical camera, which limits the scalability of 3DGS pipelines when applied to fisheye imagery in uncontrolled or large-scale data collection setups.

2.2 Fisheye Extensions of 3D Gaussian Splatting

A small number of recent works have extended 3D Gaussian Splatting to support non-linear projection models, with a focus on rendering from fisheye cameras. Huang et al. [6] propose a modified projection function that reduces distortion from the affine approximation in standard pipelines. Deng et al. [3] present a self-calibrating approach that jointly estimates intrinsics, distortion, and geometry, but do not demonstrate full fisheye rendering. Nazarenius and Kou [17] introduce a differentiable space-warping strategy for arbitrary distortion functions, though their results are limited to synthetic fisheye images. To our knowledge, only Fisheye-GS [15] and 3DGUT [21] explicitly support rendering to circular fisheye images using splatting-based methods.

Fisheye-GS replaces the perspective camera model with an equidistant projection and is among the first to render directly in the fisheye image domain. It preserves peripheral content without requiring undistortion and assumes accurate calibration. 3D Gaussian Unscented Transform (3DGUT) modifies the splatting formulation by replacing Elliptical Weighted Average (EWA) splatting

[26] with the Unscented Transform [5], which allows direct projection through non-linear camera models such as fisheye lenses. The method also accounts for effects like reflections and rolling shutter. Details about these two methods are provided in the Supplementary Material.

2.3 Learning Based Methods for Monocular Fisheye Depth Estimation

Monocular depth estimation has advanced with transformer-based models like Depth Anything V1, V2 [22,23] and MoGe [20], which leverage large-scale pre-training to predict depth from single perspective images. These models perform well across standard domains but are trained only on perspective imagery. Their predictions degrade significantly under strong radial distortion or wide FoV.

Several self-supervised methods have been proposed specifically for fisheye images. FisheyeDistanceNet [12] uses distortion-aware projection and supervision, while FisheyeDistanceNet++ [14] adds attention and a robust loss to improve accuracy. UnRectDepthNet [13] handles distortion using the unified camera model, avoiding undistortion. FisheyeDepth [25] uses externally estimated poses for improved scale consistency. These methods improve fisheye depth estimation but depend on fixed distortion models and often assume task-specific hardware setups.

UniK3D [18] is a recent transformer-based model that supports arbitrary intrinsics, including fisheye and wide-angle lenses. It introduces a spherical 3D scene representation and predicts ray distributions using a learned spherical harmonic basis. An angular supervision term enforces consistency in wide-FoV scenes. UniK3D does not require predefined distortion models and generalizes across camera types. We use UniK3D to generate depth maps and ray directions from 200° fisheye images. These are fused into dense point clouds that replace SfM initialization in 3D Gaussian Splatting. Although UniK3D has not been trained on real-world fisheye images with extreme fields of view (e.g., 200°), we assess whether its outputs are sufficiently reliable to support high-quality reconstruction with Fisheye-GS and 3DGUT, which are capable of rendering directly into circular fisheye views.

3 Method

3.1 Data and Camera Calibration

We use four scenes—two indoor, two outdoor—from the FIORD dataset [4], captured with the Insta360 One RS 1-Inch camera [7]. Each scene includes 200–400 high-resolution fisheye images. The indoor scenes contain fine-grained geometry and dense clutter. One outdoor scene includes winter conditions such as fog, snow, and glare. The other features more typical lighting and structure.

Each dual-lens capture provides two 200° fisheye views. We extract each view into a 3264×3264 PNG by splitting the side-by-side image. We calibrate each

lens independently using the Camera Calibration Toolbox for Generic Lenses [8,9]. The estimated intrinsics and radial distortion parameters are converted to OpenCV’s fisheye format and used in COLMAP’s Structure-from-Motion pipeline. Calibration accuracy is verified by rectifying input images and visually checking for projection consistency.

We use a 90/10 train-test split for all scenes. Reconstruction quality is reported on test views using PSNR, SSIM, and LPIPS [24].

3.2 Evaluated Gaussian Splatting Modules for Fisheye Cameras

We evaluate two recent splatting pipelines adapted for fisheye imagery: Fisheye-GS and 3DGUT. Both build on the 3D Gaussian Splatting (3DGS) framework but introduce modifications to support non-linear projection models. We use their official codebases and adapt both methods to work with our calibrated fisheye images. Prior to splatting, we estimate camera poses and sparse geometry using a Structure-from-Motion (SfM) pipeline.

Structure-from-Motion (SfM) We use COLMAP v3.9.1 with the OpenCV fisheye model to recover camera parameters and 3D points. Each scene is processed using intrinsics derived from calibration (fx, fy, cx, cy, k1–k4). Feature extraction is configured for high-resolution inputs by increasing the maximum image size and keypoint count. Matching is performed using the vocabulary tree matcher, followed by incremental registration and triangulation. The resulting sparse point cloud and camera poses are globally refined through bundle adjustment and exported in binary format for downstream use.

Fisheye-GS Implementation We evaluate Fisheye-GS on real 200° fisheye images captured in diverse conditions, including reflections, occlusions, and low-texture regions. Performance near the image periphery is of particular interest, as distortion is strongest there. Fisheye-GS assumes an equidistant projection and includes a preprocessing step that reprojects the input images using intrinsics and distortion coefficients from COLMAP. The implementation omits the k1 term, which models the dominant component of radial distortion in real fisheye lenses. This exclusion reflects the model’s assumption of a distortion-free equidistant projection, where radial displacement is linearly proportional to the angle of incidence. Including k1 would introduce non-linear radial warping that violates this assumption and causes inconsistencies during rendering. The equidistant model is only defined up to 180° ($\theta = \pi$). Rays beyond this limit originate from behind the optical axis and cannot be mapped consistently. Since our data spans 200°, this leads to projection ambiguity near the periphery.

3DGUT Implementation We evaluate 3DGUT on the same 200° fisheye data to assess its performance under extreme distortion. Unlike Fisheye-GS, 3DGUT directly applies the full non-linear fisheye model and does not require reprojection. It uses the Unscented Transform to project sigma points from each 3D Gaussian, avoiding local linearization and improving accuracy near the image periphery.

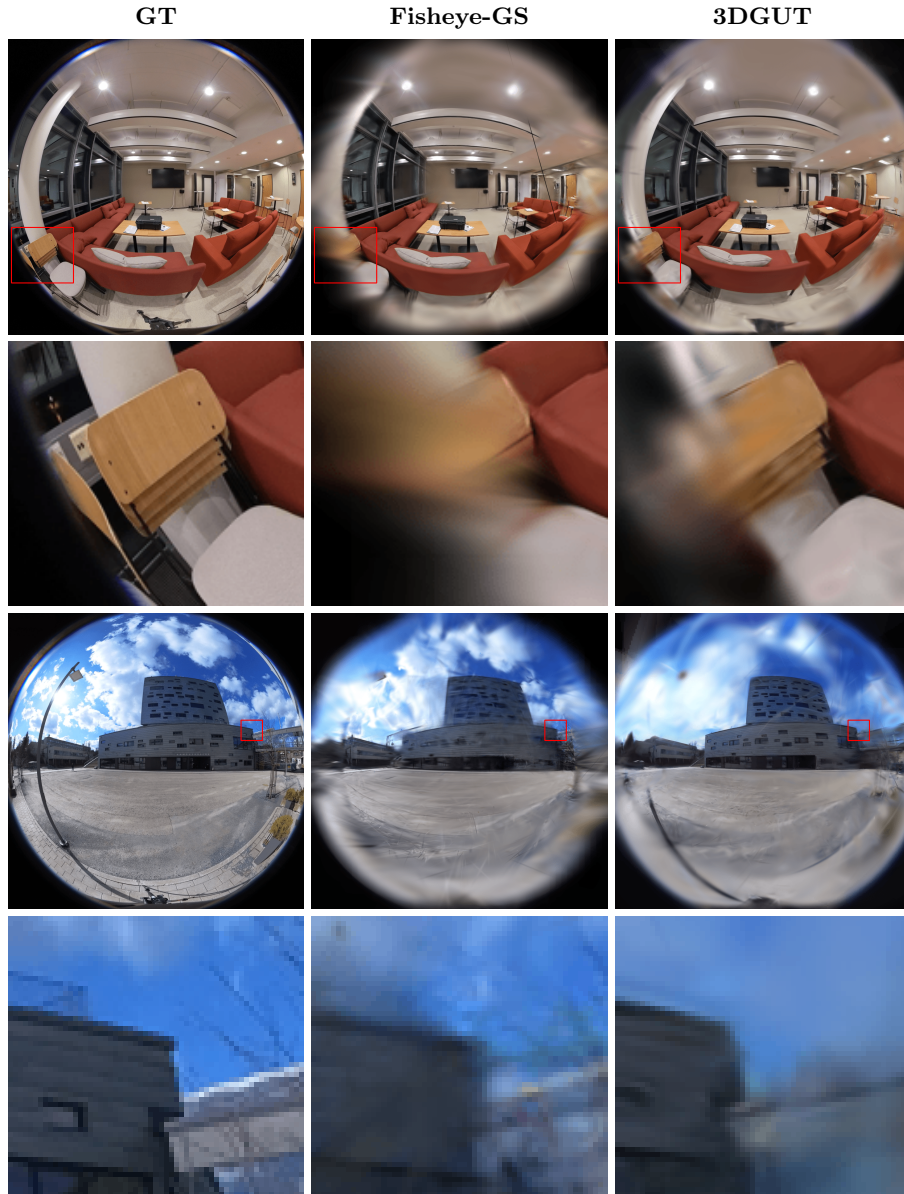


Fig. 1: Qualitative comparison of rendering results from Fisheye-GS and 3DGUT across two experimental scenes, with zoomed-in parts (marked with squares on original images). While 3DGUT introduces floaters, its distortion modeling is superior to Fisheye-GS in both indoor and outdoor settings.

We enable the optional Markov Chain Monte Carlo (MCMC) training mode

[11], which interprets Gaussians as stochastic samples and updates them using Langevin dynamics [2]. This replaces heuristic densification strategies and adaptively redistributes Gaussians in regions affected by strong distortion or sparse supervision. We use the official codebase with default settings and adapt it to our calibrated fisheye setup. The implementation supports real 200° fisheye images without projection preprocessing, which allows us to directly evaluate its robustness in wide-angle scenarios.

3.3 Field of View Adjustment

Our fisheye cameras capture 200° views, exceeding the 180° limit of the equidistant projection assumed by Fisheye-GS. Beyond this range, rays originate from behind the optical axis and cannot be projected consistently. While 3DGUT supports arbitrary camera models, both methods show sensitivity to distortion near the image boundary at wide angles.

To investigate the tradeoff between peripheral distortion and scene coverage, we generate additional image sets at 160° and 120°. Each 200° input is reprojected to the target FoV under the equidistant model by adjusting the focal length, rescaling angular coordinates, and discarding pixels beyond the desired angular range. Reprojection is implemented using OpenCV with bilinear interpolation. We apply this transformation to all images in the selected scenes and process the results through the COLMAP SfM pipeline using the OpenCV fisheye model. Each FoV variant is then used to train and evaluate both Fisheye-GS and 3DGUT to assess how reconstruction quality and rendering behavior change under reduced angular input.

3.4 Depth Estimation Based Gaussian Initialization

SfM pipelines often perform poorly on fisheye images due to distortion, sparse feature matching, and long processing times. As an alternative, we initialize the Gaussian Splatting pipeline using monocular depth maps predicted from individual fisheye views. For each scene, we select only 2–3 fisheye images to leverage one of the key advantages of fisheye cameras—the ability to capture large portions of the scene in a single frame. Each selected image is passed through UniK3D to obtain a depth map and corresponding ray directions, which are projected into a local 3D point cloud using the known intrinsics. These per-image clouds are then fused into a single dense point cloud. This minimal-view strategy also helps reduce multiview inconsistencies, as the estimator processes each image independently and does not enforce cross-view consistency.

To align the resulting point cloud with our Gaussian Splatting pipelines, we estimate a similarity transform using COLMAP camera poses and rescale the cloud accordingly. The final point cloud is expressed in COLMAP coordinates and can be used directly with both Fisheye-GS and 3DGUT, avoiding the need for traditional SfM reconstruction. Although UniK3D is not trained on real-world fisheye imagery with extreme FoV (e.g., 200°), this setup allows us to evaluate its generalization ability and assess its suitability as a source of geometry for

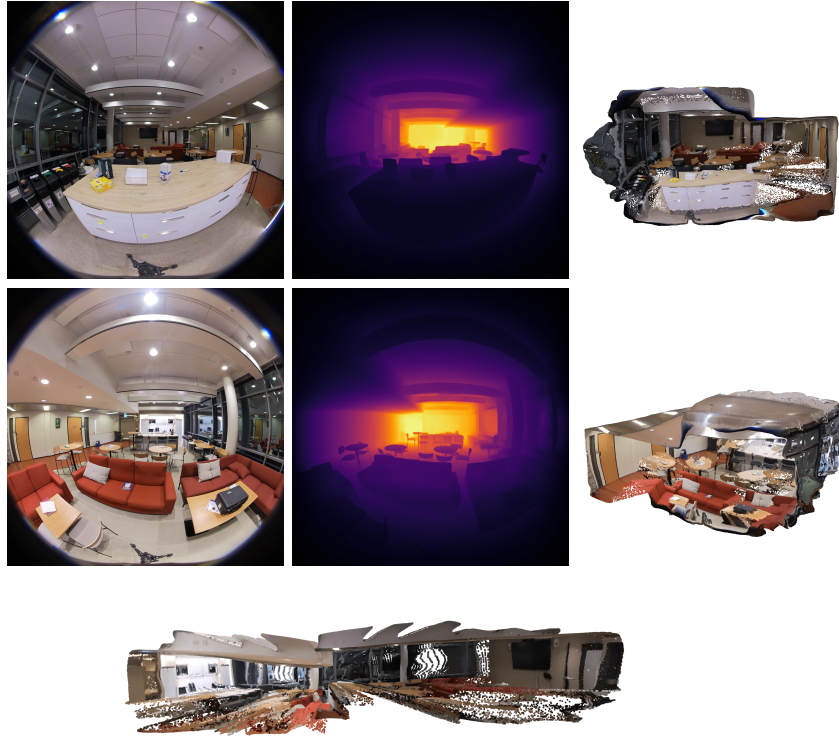


Fig. 2: Point cloud generation using UniK3D. Two fisheye views are processed to produce dense depth maps and local point clouds, which are fused via pose alignment into a single global point cloud (bottom).

direct 3D initialization. Example depth maps, monocular reconstructions, and fused point clouds are shown in Figure 2.

3.5 Training Resources

All models are trained on a single NVIDIA RTX 4090 GPU with 24 GB of memory. Fisheye-GS requires approximately 7–10 GB of GPU memory and trains in 35–50 minutes, depending on scene size and image resolution. 3DGUT uses a similar memory range but takes 60–80 minutes per scene. For experiments initialized with depth map-generated point clouds, memory usage increases to 13–18 GB for both methods due to the larger number of Gaussians. Each depth map contributes many more points than sparse SfM. In 3DGUT, this is further amplified by the Unscented Transform, which expands each Gaussian into multiple sigma points, and by MCMC-based sampling, which adds computation for densification and convergence. Despite the increased cost, both pipelines remain feasible on high-end consumer hardware.

Table 1: Quantitative comparison of Fisheye-GS and 3DGUT under different FOVs. Metrics reported: PSNR \uparrow / SSIM \uparrow / LPIPS \downarrow .

Dataset	Method	FOV = 200			FOV = 160			FOV = 120		
		PSNR \uparrow	SSIM \uparrow	LPIPS \downarrow	PSNR \uparrow	SSIM \uparrow	LPIPS \downarrow	PSNR \uparrow	SSIM \uparrow	LPIPS \downarrow
Indoor_1	Fisheye-GS	20.05	0.7238	0.3862	24.01	0.8190	0.2509	19.43	0.7713	0.2569
	3D-GUT	22.16	0.8140	0.3242	23.29	0.8621	0.2131	20.33	0.8402	0.2124
Indoor_2	Fisheye-GS	19.62	0.7008	0.4024	24.04	0.8445	0.2203	20.98	0.8314	0.2075
	3D-GUT	20.91	0.7787	0.3594	22.67	0.8783	0.1946	21.32	0.8766	0.1812
Outdoor_1	Fisheye-GS	19.86	0.6432	0.3648	20.58	0.7332	0.2527	15.75	0.6394	0.3179
	3D-GUT	20.25	0.6261	0.3385	20.35	0.7422	0.2413	16.37	0.6641	0.2745
Outdoor_2	Fisheye-GS	17.11	0.5664	0.4877	19.20	0.6539	0.3652	18.14	0.6596	0.3411
	3D-GUT	18.54	0.6479	0.4461	18.22	0.7510	0.3002	17.66	0.7375	0.2286

4 Results

4.1 Evaluation on Real Fisheye Images

Our primary goal is to evaluate how each method handles wide-FoV distortion in real-world fisheye images. 3DGUT accommodates non-linear distortions near the periphery by operating directly on raw fisheye inputs using the Unscented Transform. Fisheye-GS relies on a simplified equidistant projection and introduces warping at the fringes in 200° captures. Table 1 reports results across four scenes. We focus on the 200° FoV, which introduces the strongest distortion and reflects the full capability of our capture setup. Both methods perform similarly in PSNR, with small scene-level differences. 3DGUT scores higher in perceptual metrics such as SSIM and LPIPS. The largest differences appear near the image periphery, where projection fidelity becomes critical.

Figure 1 shows rendered test views from two scenes. 3DGUT preserves texture and object boundaries more consistently in regions affected by distortion. Scene Outdoor_1 poses challenges unrelated to method choice. Repeating floor patterns interfere with COLMAP feature matching. Fog and glare reduce image contrast. Snow-covered surfaces lack high-frequency texture. These factors reduce reconstruction quality for both methods. 3DGUT retains more coherent geometry near high-distortion areas, though the improvement over Fisheye-GS is limited in this scene. Scene Outdoor_2 shows the greatest drop in performance. The scene includes open sky and direct sunlight. Lack of textured features weakens SfM and image-based supervision. Lighting variation, overexposure, and lens flare introduce inconsistencies. Neither method compensates for these conditions. PSNR and SSIM decline across both pipelines. The results highlight limitations of splatting in low-feature, high-dynamic-range outdoor fisheye settings.

4.2 Impact of Field of View Adjustment

We evaluated both methods under reduced FoVs of 160° and 120° to study how projection distortion and scene coverage trade off in fisheye rendering. Table 1

Table 2: Evaluation of Fisheye-GS and 3D-GUT on four scenes using two initialization strategies: SfM and depth-based. Metrics: PSNR \uparrow / SSIM \uparrow / LPIPS \downarrow .

Scene	Method	Init Type	#Points	PSNR \uparrow	SSIM \uparrow	LPIPS \downarrow
Indoor_1	Fisheye-GS	SfM	82.1K	20.05	0.7238	0.3862
	3D-GUT	SfM		22.16	0.8140	0.3242
	Fisheye-GS	Depth	2.13M	19.96	0.7173	0.3928
	3D-GUT	Depth		18.76	0.754	0.3376
Indoor_2	Fisheye-GS	SfM	147K	19.62	0.7008	0.4024
	3D-GUT	SfM		20.91	0.7787	0.3594
	Fisheye-GS	Depth	2.13M	20.22	0.7226	0.3737
	3D-GUT	Depth		18.33	0.751	0.3632
Outdoor_1	Fisheye-GS	SfM	219K	19.86	0.6432	0.3648
	3D-GUT	SfM		20.25	0.6261	0.3385
	Fisheye-GS	Depth	2.13M	19.97	0.6346	0.3738
	3D-GUT	Depth		21.13	0.6394	0.3529
Outdoor_2	Fisheye-GS	SfM	140K	17.11	0.5664	0.4877
	3D-GUT	SfM		18.54	0.6479	0.4461
	Fisheye-GS	Depth	2.64M	17.02	0.5614	0.4932
	3D-GUT	Depth		16.45	0.5391	0.5156

shows that Fisheye-GS benefits noticeably from reducing the FoV to 160° , with consistent improvements in SSIM and LPIPS across all scenes. This reflects its reliance on an equidistant projection model, which becomes more stable as peripheral distortion is trimmed. At 120° , performance often drops, as the narrower field compromises scene context and reduces image content available for reconstruction. 3DGUT remains stable across FoVs, with modest changes in quantitative results. It improves slightly at 160° , and its perceptual metrics remain strong even at 120° . The method directly handles distorted input and maintains performance without needing adjustments tied to FoV or projection assumptions.

Figure 3 shows how FoV changes affect visual quality and scene coverage for both methods on the Outdoor_1 scene. Trimming the FoV improves projection consistency but discards peripheral content, which can reduce useful context. This tradeoff is especially relevant in wide-angle applications where coverage is as important as distortion handling. Fisheye-GS improves clearly when reduced from 200° to 160° , but shows reduced quality at 120° , where input content becomes too limited for stable results. 3DGUT remains robust across all tested FoVs. In outdoor scenes with complex lighting, reduced FoV occasionally introduces floaters. These artifacts appear in regions with fog or strong sunlight, where limited context from the narrower view makes it harder to resolve visibility and depth relationships.

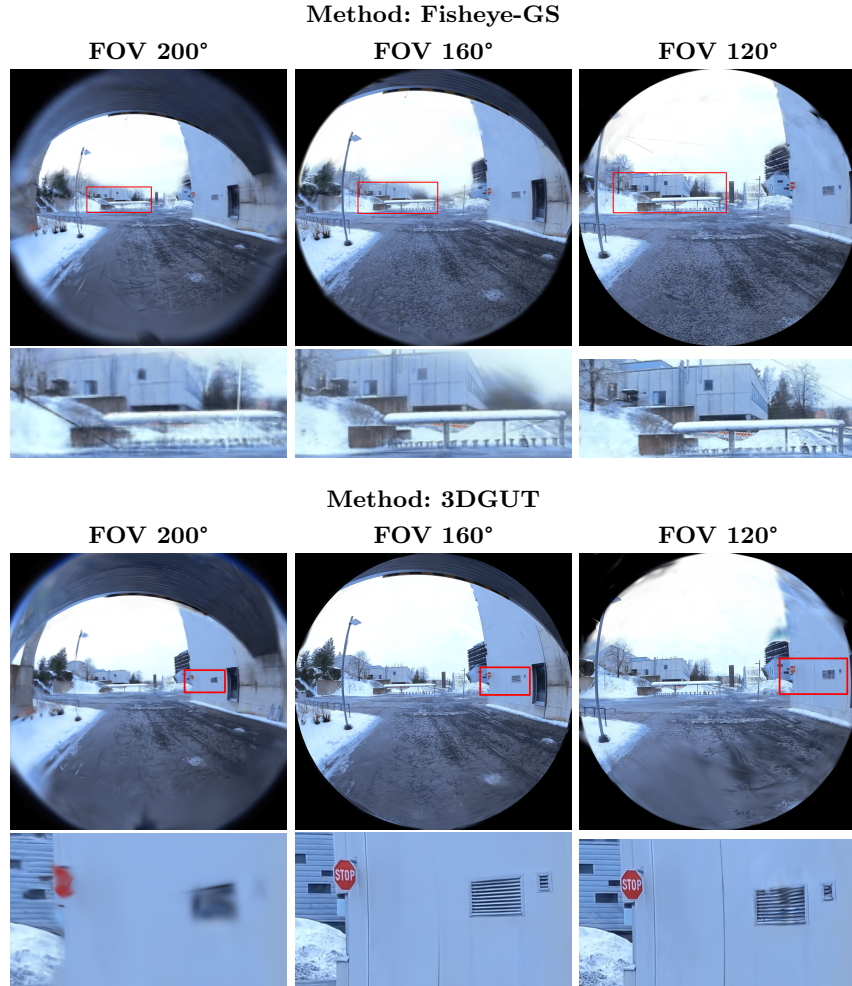


Fig. 3: Effect of FoV reduction on Outdoor_1 renderings. Narrower FoVs crop more input content; 160° provides a good balance between coverage and quality.

4.3 Impact of Depth-Based Initialization

Table 2 reports results using monocular depth-based initialization versus SfM for Fisheye-GS and 3DGUT. Performance is comparable despite using only 2–3 fisheye views per scene. Depth-based initialization avoids the cost of SfM while achieving similar reconstruction quality. The resulting point clouds are denser, increasing memory slightly but improving scene coverage. For Fisheye-GS, differences are small. Indoor_2 sees slight gains in PSNR and LPIPS; other scenes remain stable. Denser input yields more Gaussian primitives and can offer more detail. Since the depth is predicted independently and the fused cloud is scaled

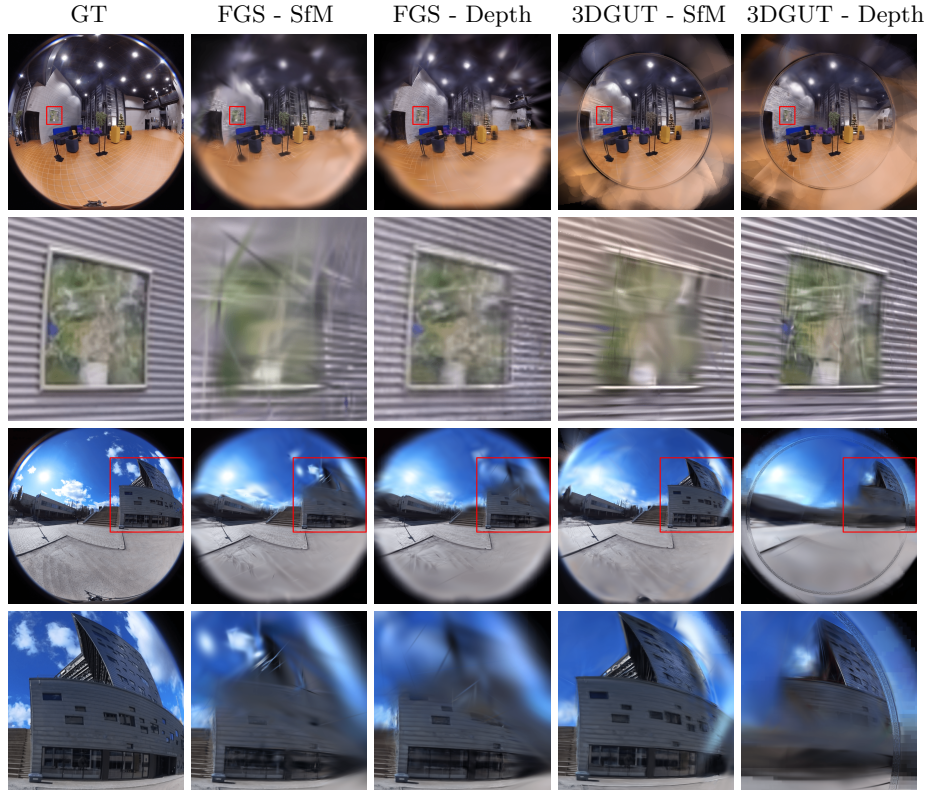


Fig. 4: Comparison of example rendered outputs from Indoor_2 and Outdoor_2 using different initialization strategies (FGS: Fisheye-GS).

and aligned to COLMAP poses, some misalignment between the point cloud and the camera poses is expected, though it does not visibly degrade results.

3DGUT shows more variation. Outdoor_1 improves with depth-based input, while Indoor_2 and Outdoor_2 degrade modestly. Gaussians are not explicitly relocated or pruned but are optimized over time. Dense input can lead to sub-optimal configurations in unstructured scenes with uncertain depth. Despite this, monocular depth remains a practical alternative to SfM for wide-FoV reconstruction. It performs best in detailed, distortion-heavy regions (Figure 4). Outdoor scenes often contain distant or low-texture areas that are harder to initialize. Indoor scenes are more structured and consistent. Balancing density and coverage is essential. These findings highlight the importance of depth quality and spatial alignment when replacing SfM.

5 Conclusion

We conducted the first evaluation of 3D Gaussian splatting on real fisheye imagery with fields of view of more than 180° . Fisheye-GS and 3DGUT were tested in indoor and outdoor scenes with 200° cameras. Both methods handled distortion reliably. Fisheye-GS improved at 160° , but degraded at 120° . 3DGUT remained stable across FoVs but showed floaters in reduced views and complex lighting. We replaced SfM with monocular depth from 2–3 fisheye images. The resulting point clouds matched SfM quality and aligned with the COLMAP frame. Inefficiencies appeared in outdoor scenes with unstructured geometry. These results support the use of wide-FoV imagery without any preprocessing requirements and depth-based initialization in reconstruction pipelines.

References

1. Bradski, G.: The OpenCV Library. *Dr. Dobb's Journal of Software Tools* (2000)
2. Brosse, N., Durmus, A., Moulines, E.: The promises and pitfalls of stochastic gradient langevin dynamics (2018), <https://arxiv.org/abs/1811.10072>
3. Deng, Y., Xian, W., Yang, G., Guibas, L., Wetzstein, G., Marschner, S., Debevec, P.: Self-calibrating gaussian splatting for large field of view reconstruction (2025), <https://arxiv.org/abs/2502.09563>
4. Gunes, U., Turkulainen, M., Ren, X., Solin, A., Kannala, J., Rahtu, E.: Fiord: A fisheye indoor-outdoor dataset with lidar ground truth for 3d scene reconstruction and benchmarking. In: SCIA (2025)
5. Gustafsson, F., Hendeby, G.: Some relations between extended and unscented kalman filters. *Signal Processing, IEEE Transactions on* **60**, 545 – 555 (03 2012). <https://doi.org/10.1109/TSP.2011.2172431>
6. Huang, L., Bai, J., Guo, J., Li, Y., Guo, Y.: On the error analysis of 3d gaussian splatting and an optimal projection strategy (2024), <https://arxiv.org/abs/2402.00752>
7. Insta360: Insta360 One RS 1-Inch 360 Edition Specifications (2024), <https://www.insta360.com/product/insta360-oners/1inch-360>
8. Kannala, J., Brandt, S.: A generic camera model and calibration method for conventional, wide-angle, and fish-eye lenses. *IEEE Transactions on Pattern Analysis and Machine Intelligence* **28**(8), 1335–1340 (2006). <https://doi.org/10.1109/TPAMI.2006.153>
9. Kannala, J., Heikkilä, J., Brandt, S.S.: Geometric camera calibration. *Wiley encyclopedia of computer science and engineering* **13**(6), 1–20 (2008)
10. Kerbl, B., Kopanas, G., Leimkühler, T., Drettakis, G.: 3d gaussian splatting for real-time radiance field rendering. *ACM Transactions on Graphics* **42**(4) (July 2023), <https://repo-sam.inria.fr/fungraph/3d-gaussian-splatting/>
11. Kheradmand, S., Rebain, D., Sharma, G., Sun, W., Tseng, J., Isack, H., Kar, A., Tagliasacchi, A., Yi, K.M.: 3d gaussian splatting as markov chain monte carlo (2025), <https://arxiv.org/abs/2404.09591>
12. Kumar, V.R., Hiremath, S.A., Bach, M., Milz, S., Witt, C., Pinar, C., Yogamani, S., Mäder, P.: Fisheyedistancenet: Self-supervised scale-aware distance estimation using monocular fisheye camera for autonomous driving. In: 2020 IEEE International Conference on Robotics and Automation (ICRA). pp. 574–581 (2020). <https://doi.org/10.1109/ICRA40945.2020.9197319>
13. Kumar, V.R., Yogamani, S., Bach, M., Witt, C., Milz, S., Mader, P.: Unrectdepthnet: Self-supervised monocular depth estimation using a generic framework for handling common camera distortion models (2023), <https://arxiv.org/abs/2007.06676>
14. Kumar, V.R., Yogamani, S.K., Milz, S., Mäder, P.: Fisheyedistancenet++: Self-supervised fisheye distance estimation with self-attention, robust loss function and camera view generalization. In: *Autonomous Vehicles and Machines*. pp. 1–11 (2021), <https://doi.org/10.2352/ISSN.2470-1173.2021.17.AVM-181>
15. Liao, Z., Chen, S., Fu, R., Wang, Y., Su, Z., Luo, H., Ma, L., Xu, L., Dai, B., Li, H., Pei, Z., Zhang, X.: Fisheye-gs: Lightweight and extensible gaussian splatting module for fisheye cameras (2024), <https://arxiv.org/abs/2409.04751>
16. Mildenhall, B., Srinivasan, P.P., Tancik, M., Barron, J.T., Ramamoorthi, R., Ng, R.: Nerf: Representing scenes as neural radiance fields for view synthesis. In: *ECCV* (2020)

17. Nazarenius, J., Kou, S., Zhang, F.L., Koch, R.: Arbitrary optics for gaussian splatting using space warping. *Journal of Imaging* **10**(12) (2024). <https://doi.org/10.3390/jimaging10120330>, <https://www.mdpi.com/2313-433X/10/12/330>
18. Piccinelli, L., Sakaridis, C., Segu, M., Yang, Y.H., Li, S., Abbeloos, W., Van Gool, L.: UniK3D: Universal camera monocular 3d estimation. In: *IEEE/CVF Conference on Computer Vision and Pattern Recognition (CVPR)* (2025)
19. Schönberger, J.L., Frahm, J.M.: Structure-from-motion revisited. In: *Conference on Computer Vision and Pattern Recognition (CVPR)* (2016)
20. Wang, R., Xu, S., Dai, C., Xiang, J., Deng, Y., Tong, X., Yang, J.: Moge: Unlocking accurate monocular geometry estimation for open-domain images with optimal training supervision (2024), <https://arxiv.org/abs/2410.19115>
21. Wu, Q., Martinez Esturo, J., Mirzaei, A., Moenne-Loccoz, N., Gojcic, Z.: 3dgt: Enabling distorted cameras and secondary rays in gaussian splatting. *Conference on Computer Vision and Pattern Recognition (CVPR)* (2025)
22. Yang, L., Kang, B., Huang, Z., Xu, X., Feng, J., Zhao, H.: Depth anything: Unleashing the power of large-scale unlabeled data. In: *CVPR* (2024)
23. Yang, L., Kang, B., Huang, Z., Zhao, Z., Xu, X., Feng, J., Zhao, H.: Depth anything v2. *arXiv:2406.09414* (2024)
24. Zhang, R., Isola, P., Efros, A.A., Shechtman, E., Wang, O.: The unreasonable effectiveness of deep features as a perceptual metric (2018), <https://arxiv.org/abs/1801.03924>
25. Zhao, G., Liu, Y., Qi, W., Ma, F., Liu, M., Ma, J.: Fisheyedepth: A real scale self-supervised depth estimation model for fisheye camera (2024), <https://arxiv.org/abs/2409.15054>
26. Zwicker, M., Pfister, H., van Baar, J., Gross, M.: Ewa splatting. *IEEE Transactions on Visualization and Computer Graphics* **8**(3), 223–238 (07/2002-09/2002 2002)